# Absolute cross sections for the $^{12}C(\pi^{\pm},\pi N)^{11}C$ reactions between 40 and 600 MeV

B. J. Dropesky, G. W. Butler, C. J. Orth, R. A. Williams, and M. A. Yates-Williams
*Los Alamos Scientific Laboratory, University of California, Los Alamos, New Mexico 87545*

G. Friedlander
*Chemistry Department, Brookhaven National Laboratory, Upton, New York 11973*

S. B. Kaufman
*Chemistry Division, Argonne National Laboratory, Argonne, Illinois 60439*

(Received 27 March 1979)

The excitation functions for the $^{12}C(\pi^{\pm},\pi N)^{11}C$ reactions have been established for 40- to 600-MeV $\pi^-$ and 50- to 520-MeV $\pi^+$. These excitation functions are dominated by the (3,3) pion-nucleon resonance but show an upward energy shift in the resonance peak for $\pi^-$ (to about 190 MeV) and a downward shift for $\pi^+$ (to about 160 MeV). The $\sigma(\pi^-)/\sigma(\pi^+)$ ratio at 180 MeV is $1.59\pm0.07$. The results are compared with theoretical calculations based on a semiclassical transport model including nucleon charge exchange and an intranuclear cascade model.

[NUCLEAR REACTIONS $^{12}C(\pi^{\pm},\pi N)^{11}C$, excitation functions, $E\pi^+ = 50-520$ MeV, $E\pi^- = 40-600$ MeV. Plastic scintillator targets, measured $^{11}C$ by $\beta^+-\gamma$ coincidences. Compared with semiclassical transport and intranuclear cascade calculations.]

## I. INTRODUCTION

With the advent of the so-called "meson factories" and their intense pion beams it became necessary to develop activation techniques to measure the pion fluxes because it would no longer be possible to count individual particles by electronic methods, and the use of current integrating devices would be impractical for most activation studies. For the same reasons that the $^{12}C(p,pn)^{11}C$ reaction served as the basis for foil activation techniques for monitoring proton beams, the corresponding reactions with pions, $^{12}C(\pi^{\pm},\pi N)^{11}C$, were selected.[1] These reasons are (a) the conveniently short 20.4-m half-life of $^{11}C$, (b) the relatively large cross sections for these reactions, and (c) the ease with which the absolute disintegration rate of the $^{11}C$ induced in a plastic scintillator could be determined. Therefore, at pion particle rates low enough to be determined with electronic counting techniques sufficient amounts of $^{11}C$ could be produced to determine accurately the reaction cross sections. The resultant cross sections for $^{11}C$ production by pion interactions with carbon then enable one to utilize this activation technique to be applied as a primary beam monitor.

The first important use of these cross sections is for establishing the excitation functions of more practical secondary monitor reactions that are essential for carrying out a wide variety of activation studies where irradiations longer than an hour are required. These monitor reactions involve the production of 110-m $^{18}F$ and 15-h $^{24}Na$ from Al and Si with both $\pi^+$ and $\pi^-$ and the measurement of their cross sections relative to the $^{12}C(\pi^{\pm},\pi N)^{11}C$ reaction cross sections. They have distinct advantages over the carbon monitor due to the longer half-lives of the measured activities and the smaller variation of cross sections with energy. The excitation functions of these secondary pion beam monitor reactions are being determined and will be reported separately.

An equally important reason for studying the reactions in carbon stemmed from the considerable theoretical interest aroused by the reported ratio of about unity[2] for the $\pi^-$ to $\pi^+$ neutron knock-out cross sections on $^{12}C$ at the (3,3) resonance (180 MeV). On the basis of the free-particle pion-nucleon cross sections and a simple nucleon knock-out model, a $\sigma(\pi^-)/\sigma(\pi^+)$ ratio $R$ near 3 had been predicted. Several attempts were made to explain this discrepancy by such concepts as "quasi-alpha particles,"[3] excitation of intermediate isospin states,[2-4] Fermi averaging,[5,6] compound nucleus effects,[7] and formation of nucleon isobars and charge exchange,[8] but none of these could explain an $R$ value of unity. However, this last approach[8] came close to accounting for the value of $R$ as determined in the present study.

Prior to this work, a credible determination of the excitation function of the $^{12}C(\pi^-,\pi N)^{11}C$ reaction, at fairly large energy intervals across the (3,3) resonance, was reported by Reeder and

Markowitz.[9] For $\pi^+$, however, serious discrepancies existed among the reported cross-section measurements,[2,9-12] especially above 120 MeV. Therefore, it was considered essential that a thorough remeasurement of these excitation functions be made in order to resolve these discrepancies.

The present study was carried out during the early operating phase of the Clinton P. Anderson Meson Physics Facility (LAMPF) when the pion beam intensities were low. We have determined the excitation functions of the $^{12}C(\pi^{\pm},\pi N)^{11}C$ reactions over the entire useful energy range available at LAMPF (≈40–600 MeV), and a preliminary report of our results has been published.[13] Soon after these early results appeared, a group at Leningrad reported[14] their cross-section measurements for the $^{12}C(\pi^{\pm},\pi N)^{11}C$ reactions over the energy range 100 to 300 MeV, using basically the same techniques employed in the present study. While their $\sigma(\pi^-)/\sigma(\pi^+)$ ratios agree well with ours, their cross sections are somewhat higher than ours above the (3, 3) resonance.

Additional measurements have been made since our earlier publication[13] and the final results and details of the experimental procedures and data analyses are reported here.

## II. EXPERIMENTAL

### A. Pion channels and beam tuning

The pion beams used for this study were obtained from two different channels at LAMPF: LEP (Low Energy Pion channel) and $P^3$ (Particle and Pion Physics channel) for high-energy pions. These channels are described in detail in Refs. 15 and 16, respectively. The range of energies selected on the LEP channel was about 40 to 180 MeV. On the $P^3$ channel, $\pi^-$ energies from 100 to 600 MeV and $\pi^+$ energies from 100 to 520 MeV were used. Both channels were tuned so as to produce a waist in the beam at the target position such that at least 99% of the beam was within the 3.8-cm diameter of the target disks, thus eliminating any error due to misalignment of target and counter telescope. The momentum spread ($\Delta P/P$) transmitted by each channel was kept as low as possible consistent with the intensity desired; this spread was usually 1 to 2% on LEP and 2 to 4% on $P^3$. (For 600-MeV $\pi^-$, a $\Delta P/P$ of ≈6% was required to obtain sufficient pion intensity.) Removal of protons from the $\pi^+$ beams in the $P^3$ channel was accomplished by differential energy degradation of the particles. At high energies (above ≈400 MeV), protons could not be completely removed from the beam but the fraction remaining could be measured by time-of-flight (TOF) techniques. The final step before irradiating a target was to expose a Polaroid film (High Speed Type 57) to the beam to ascertain the exact position of the beam spot to ensure that the target was properly aligned.

### B. Beam particle counting

A three-element scintillation counter telescope was used to determine the pion flux incident on the target during these experiments. The telescope placement varies from 0.8 to 1.6 m from the end of the exit quadrupole magnet of the channel. A schematic diagram of the scintillation counter telescope system is shown in Fig. 1. The counter telescope consisted of three Pilot $U$ (Ref. 17) plastic scintillator disks 0.32 cm thick and spaced about 0.5 cm apart. The three circular scintillators had diameters of 3.8, 4.6, and 4.6 cm, respectively, and were coupled via Lucite light guides to RCA 31016$F$ photomultipliers. The photomultipliers, operated at 1500 $V$, put out a fast pulse (~1 nsec rise time) of 1 $V$ amplitude for a minimum ionizing particle. The three scintillation counters were oriented with their light guides 90° from each other to minimize coincidences caused by the Čerenkov radiation produced by beam particles passing through the light guides.

The electronics consisted of 300-MHz MECL III (Ref. 18) leading-edge discriminators, majority logic, and decade prescalers followed by conventional fast scalers. A high-voltage plateau curve was determined for each counter in order to establish a satisfactory operating voltage. Three quantities were recorded throughout these experiments: $C_1C_2C_3$ triple coincidences, $C_1\tilde{C}_2$ delayed coincidences, and $C_1$ singles. The coincidence delay curve for any two scintillators had a full width at half maximum (FWHM) ($2\tau$) of 6.5 nsec. This was the minimum resolving time obtainable without significant loss of counting efficiency. The triple coincidence rates were used to determine the total particle fluence. In order to determine accidental coincidence losses, the $C_1\tilde{C}_2$ rate was measured with a delay of about 50 nsec between $C_1$ and $C_2$; this delay was set so that it was an even multiple of the 5 nsec spacing of the micropulses of the main proton beam.

The total particle rate can, in principle, be determined from the $C_1C_2C_3$ and $C_1\tilde{C}_2$ rates, the separation between micropulses in the time-structured pion beam (5 nsec at LAMPF), and the resolving time of the coincidence circuit. (The Appendix describes how this can be done in detail and also defines the terms used below.) In this study, however, there were two indications that the formulas in the Appendix could not be applied

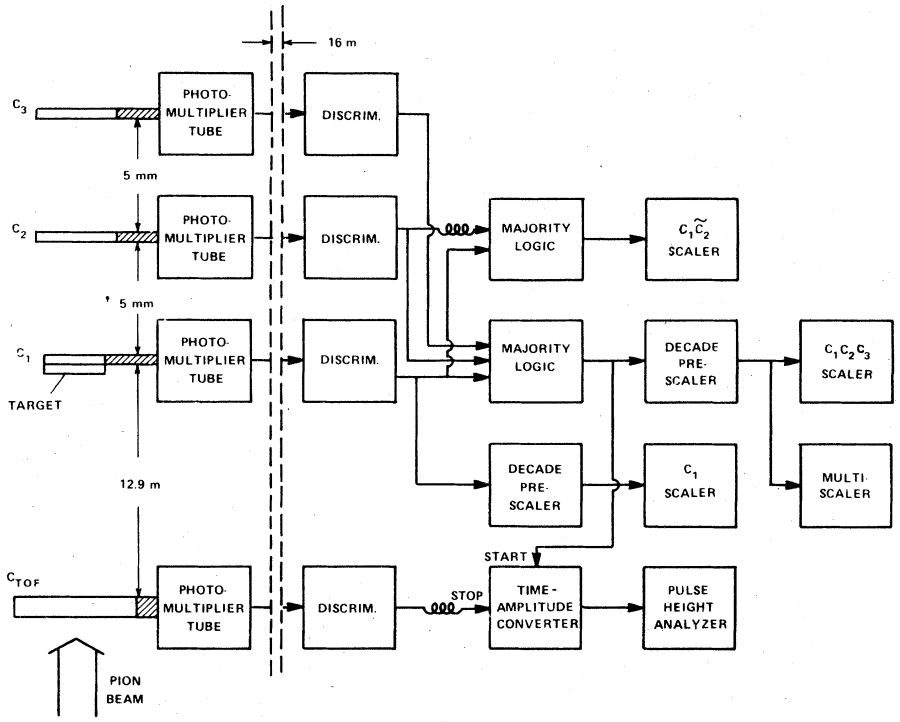


FIG. 1. Schematic diagram of counter telescope and electronics.

in a straightforward manner. First, experiments with a double pulser demonstrated that our electronics could not always separate pulses 5 nsec apart. Although the resolving time $\tau$ was about 3.3 nsec ($2\tau$ = FWHM = 6.5 nsec), other experiments showed that pion beam pulses "5 nsec" apart were detected only about half the time. This was due to the fact that the 0.25-nsec width of the proton micropulses is considerably broadened by the momentum dispersion of the pion beam so that pulses in adjacent bursts could actually be separated by anywhere from 2 to 8 nsec. Secondly, four measurements of a given cross section, made at widely different pion intensities (see Table I), showed that both the one-bunch and two-bunch resolution formulas yielded cross sections which varied with pion intensity, indicating that neither form was correct. Our solution, which brought these four measurements into closer agreement and also reflected the 0.5 probability of detecting pulses "5 nsec" apart, was to use the arithmetic average (see Sec. III B) of the rates calculated with the one- and two-bunch formulas:

$$N_p = \frac{N^2}{2N_s}\left(\ln\left(\frac{N}{N-N_s}\right) + \ln\left\{\frac{2}{1 \pm 1 - [4(N_s/N)]^{1/2}}\right\}\right).$$

TABLE I. Dependence of cross section on particle counting rate and accidental coincidence correction formula.

| | Particle rate ($\sec^{-1} \times 10^{-3}$) | | | Cross section (mb) | | |
|---|---|---|---|---|---|---|
| Run | 1-bunch[a] | 2-bunch[b] | average | 1-bunch[a] | 2-bunch[b] | average[c] |
| 117 | 714 | 868 | 791 | 45.3 | 37.3 | 40.9 |
| 118 | 34.5 | 34.8 | 34.6 | 39.7 | 39.4 | 39.5 |
| 119 | 145 | 150 | 147 | 39.7 | 38.4 | 39.1 |
| 120 | 315 | 338 | 326 | 42.3 | 39.5 | 40.8 |

[a] See Appendix, Eq. (A4).
[b] See Appendix, Eq. (A7).
[c] The average cross sections were calculated using the average particle rates.

The other complication resulted from the fact that some efficiency was sacrificed in an effort to count high particle rates successfully. A determination of the variation in the $C_1C_2C_3$ efficiency as a function of discriminator output width showed that under our operating conditions the counting efficiency was 96%. All $C_1C_2C_3$ rates were therefore increased by 4% before being used in the above formula. In the actual measurements, the beam intensity was low enough that the difference between the rates calculated with the one- and two-bunch formulas was rarely more than 2% of the $C_1C_2C_3$ rate; thus these corrections did not introduce any significant uncertainties in the final cross section.

The beam intensity was monitored continuously during each target irradiation by recording the triple coincidence counts in each 10- or 20-sec interval with a multichannel analyzer operating in the multiscaling mode. In most runs the beam intensity was constant, but for some the measured intensity fluctuations required small corrections (<3%) to be made to the apparent flux.

### C. Beam composition

The fraction of contaminant particles in the pion beams ($\mu^{\pm}, e^{\pm}, p$) was determined by two different techniques: $dE/dx$ and time of flight (TOF). For the irradiations made on the shorter LEP channel at energies below 100 MeV, the composition was determined solely by the $dE/dx$ technique; space limitations precluded the installation of an upstream scintillator for TOF measurements. The relative intensities of pions, muons, and electrons were therefore determined by their different energy losses in a plastic scintillator (25-mm thick × 50-mm diam.) which was placed at the target location. The pulse spectra from this scintillator were recorded with a pulse-height analyzer. Above 50 MeV it was necessary to insert energy degraders just upstream of the $dE/dx$ scintillator in order to resolve the three components.

A representative $dE/dx$ spectrum is shown in Fig. 2. Most of these spectra were difficult to analyze due to the variable non-Gaussian peak shapes and the unpredictable spectral continuum. Three methods of separating and integrating the peaks in these spectra were utilized: first, a hand analysis was attempted by arbitrarily drawing curves through the data and estimating the placement of the electron and muon peaks; the second method was to fit Gaussian shapes to the peaks using a general nonlinear least squares fitting program, ORGLS[19]; and lastly, SAMPO,[20] a code designed for analyzing x-ray and gamma spectra, was used to determine peak areas. These

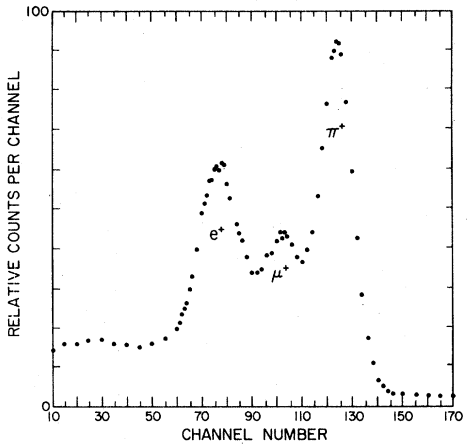


FIG. 2. Representative $dE/dx$ spectrum for 50-MeV $\pi^+$. Analysis of this type of spectrum was used to determine the pion content of beams from the low energy pion channel (LEP).

methods usually agreed to within 10% (relative), but agreement between spectra taken at the same energy but at different times was sometimes poor. Where such multiple measurements existed, a sample standard deviation was computed and expressed as a relative uncertainty. These values of the beam composition expressed as percent pions are shown in Fig. 3 as a function of pion kinetic energy. The curves are quadratic least squares fits to the data; the bands along each

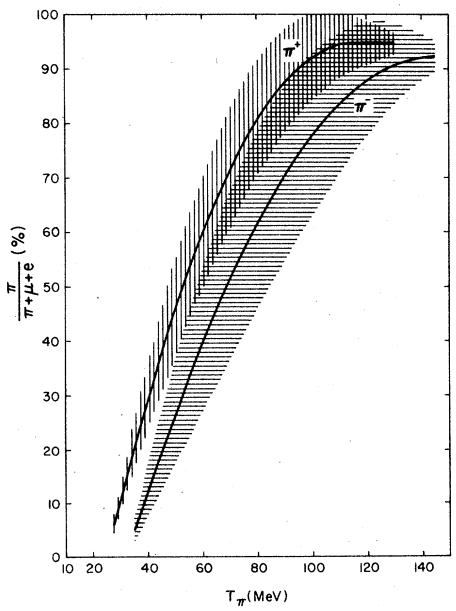


FIG. 3. Measured beam purity of the low energy pion channel. The solid curves are quadratic least squares fits to the measured values. The dashed areas indicate the limits of uncertainty.

curve result from a smoothed function of the variation of uncertainty in the composition with energy. The data were augmented by points derived from information in the LAMPF Handbook at energies too high for us to determine the beam composition. The curves thus determined (see Fig. 3) were then used in the calculation of those cross sections which were measured using the LEP channel. Calculated uncertainties generally follow the width of the bands in Fig. 3 except for those energies (notably 50 MeV) where multiple measurements of the beam composition permitted a smaller value of the uncertainty to be used.

On the $P^3$ channel the composition of the beam was determined by the TOF method. For this purpose a thin plastic scintillator was located in the channel 13 m upstream of the counter telescope. Delayed pulses from this scintillator provided the time-to-amplitude converter (TAC) stop signal while a three-fold logic output from the telescope provided the TAC start pulse (see Fig. 1). The TAC output was recorded in a pulse height analyzer. A representative TOF spectrum taken at 107 MeV is shown in Fig. 4.

All TOF spectra were analyzed using ORGLS.[19] Peaks in the spectra were each fitted with a general Gaussian function,

$$y = y_0 \exp - (x - x_0)^2 / b_0 ,$$

where the height $y_0$, position $x_0$, and width parameter $b_0$ were allowed to vary freely. The background under the peaks was fitted with a straight line, adding two more free parameters. For spectra in which there were three peaks, all eleven parameters (three for each peak plus two for the background) were varied simultaneously. The result was then plotted and compared to the original data and the program was rerun if necessary to improve the fit. The uncertainties in the fitted parameters, as determined by ORGLS, were used to determine the uncertainties in the integrated peak areas.

The curves in Fig. 5 are representative of the beam purities obtained, but the actual values used for cross-section computation were determined from the TOF spectra taken immediately before or after each target irradiation.

From the beam composition plots for the LEP and $P^3$ channels as presented in Figs. 3 and 5, respectively, it can be seen that in both channels the $\pi^+$ beams are purer than the $\pi^-$ beams, reflecting the larger yield of the former from the pion production targets. The asymptotic value of 4% muons remaining at high energy is based upon extrapolation of the data and upon preliminary Monte Carlo particle transport calculations[21] of muon contributions to the focused pion beam. This muon contribution will vary with the activation target diameter and location along the beam axis (due to pion decay), slit settings, the amount of momentum degrader in the channel, and the elemental composition of the pion production target. Therefore, these plots only describe the beam composition encountered under the specific conditions of the

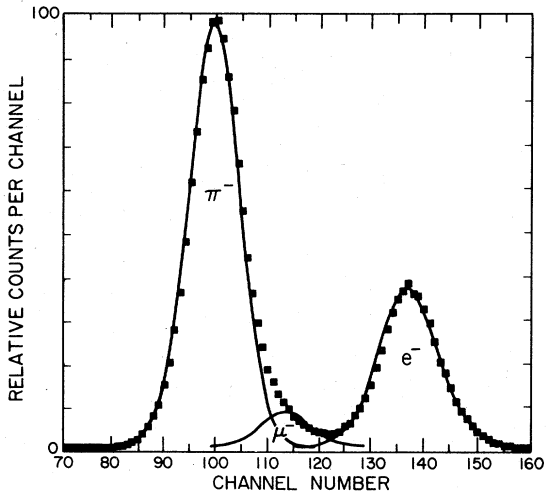


FIG. 4. Representative TOF spectrum for 107-MeV $\pi^-$. The solid curves are Gaussian least squares fits. Analysis of this type of spectrum was used to determine the purity of pion beams from the $P^3$ channel.

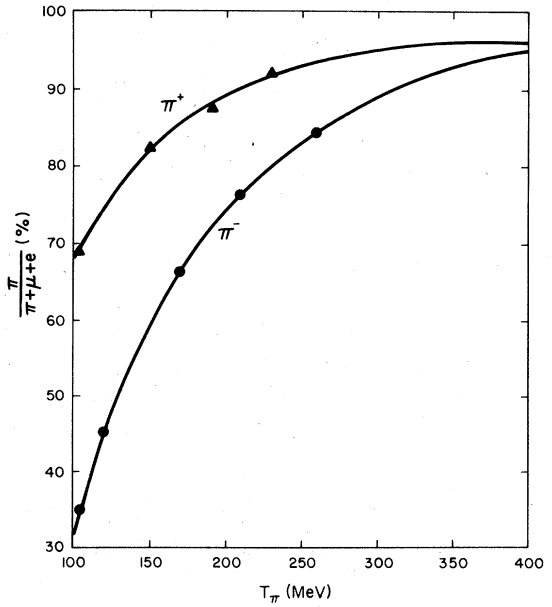


FIG. 5. $P^3$ channel beam purity as determined by TOF measurements and calculated asymptotic values of of muon contamination. Proton contamination at high $\pi^+$ energies is not included. The solid curves are drawn to aid the eye.

present work.

Proton contamination in the $\pi^+$ beam of the $P^3$ channel is a problem above ≈400 MeV where removal of the rapidly increasing number of protons by differential momentum degradation becomes less effective. However, due to the slower velocity and greater energy-loss rate of the protons relative to the pions, their contribution to the beam intensity could be determined by both TOF and $dE/dx$ techniques. In this work, both methods were used for the $\pi^+$ cross section measurements made at 340 MeV and above. Measurements above 520 MeV were not made for $\pi^+$ because the beam contained >19% protons even with 115 mm of interposed graphite momentum degraders.

A source of systematic uncertainty in the $dE/dx$ and TOF measurements was from slit scattering and the resultant enchancement of electrons in the pion beam. The occasional lack of agreement among duplicate electron contamination measurements on LEP is an indication of the magnitude of this uncertainty. Due to electronic limitations on the particle rates usable for the $dE/dx$ and TOF measurements, the beam intensity had to be reduced by at least an order of magnitude from the intensity required during the target irradiation; this reduction was achieved by narrowing the channel slits. Ideally the slits should be left in the same position as they were during the target irradiation, and the $dE/dx$ spectra should be recorded at reduced proton intensity on the pion production target. However, during most runs this was not feasible because of the simultaneous multiuse operation of the accelerator. Scattering was kept to a minimum by adjusting only the mid-channel slits.

### D. $^{11}C$ production and determination

#### 1. *Targets and irradiations*

The targets were 3.2-mm thick by 38-mm diameter disks of Pilot $B^{17}$ plastic scintillator containing 91.6% carbon by weight. These disks were the same diameter as the first scintillator ($C_1$) of the counter telescope and were taped to its upstream face during the irradiations. Precise alignment of the target and scintillator disks was ensured by a positioning cradle mounted to the light pipe of $C_1$. No correction was made for the 1.11% $^{13}C$ content of the carbon; that is, the results given in this paper technically apply to natural carbon. Also, no correction was made for loss by diffusion of $^{11}C$ from the irradiated plastic targets since this effect is negligible for such thick targets.[22] The targets were irradiated for about 30 min in beams with intensities ranging from (5 to 50) × $10^4$ particles per second. Two or more determinations were made at most energies, at beam intensities that differed by at least a factor of 2, to establish that there was no rate dependence in our procedure.

#### 2. $^{11}C$ *counting*

After each irradiation, the target was transported to the counting room where it was coupled to the face of a Dumont 6292 photomultiplier tube with optical coupling compound. An aluminum foil reflector was placed over the scintillator target and both were held in place on the end of the photomultiplier by a special cap with a 1.6-mm thick copper plate which ensured that all positrons were annihilated as close as possible to the scintillator disk. Black tape was used both to hold the cap in place and to render the assembly light-tight. This assembly was then placed in contact with the face of a 75-mm thick × 75-mm diameter NaI(Tl) scintillator inside a lead shield.

The $^{11}C$ positrons were self-detected by the plastic scintillator, and the annihilation quanta were detected in the NaI(Tl) detector which had an electronic window set to include only 511-keV photopeak pulses. Each sample was counted for at least three half-lives using standard $\beta$-$\gamma$ coincidence circuitry. The $^{11}C$ disintegration rate was calculated from the net $\beta^+$, $\gamma$, and $\beta^+$-$\gamma$ coincidence rates.[23] The data were fitted to a one-component exponential with a 20.4-min half-life using the CLSQ (Ref. 24) decay code. No significant deviations were observed from the 20.4-min half-life.

#### 3. *Proton-induced activity*

Above 300 MeV the increasing fraction of protons in the $\pi^+$ beam contributed to $^{11}C$ formation via the $^{12}C(p,pn)^{11}C$ reaction. The cross section for this reaction varies from 65 to 40 mb (Ref. 25) over the range of 90- to 180-MeV protons which have the same magnetic rigidity as 300- to 520-MeV pions. The $^{12}C(\pi^+,\pi N)^{11}C$ cross sections were calculated with appropriate corrections for the known $(p,pn)$ cross sections and our measured values of the proton contamination. See Sec. III B.

#### 4. *Possible sources of* $^{11}C$ *enhancement*

The effect of target thickness on the possible enhancement of $^{11}C$ production due to secondary particles was examined by carrying out two comparative sets of measurements with 150-MeV $\pi^+$ and 230-MeV $\pi^-$ on 3-mm and 20-mm thick scintillator targets. Since the measured $^{11}C$ activity per unit thickness showed less than 5% variation for the two thicknesses, we conclude that the tar-

get thickness effect is negligible for our 3-mm targets.

Possible contribution to the $^{11}C$ activation by background neutrons via the $^{12}C(n,2n)^{11}C$ reaction was examined on numerous occasions at both pion channels by counting thick secondary scintillator targets that had been placed near the primary target, but 5 to 10 cm outside of the beam. In all cases the secondary particle production of $^{11}C$ amounted to less than 0.5% of the activity induced by the pions.

The question of the contribution to $^{11}C$ production by inelastic lepton reactions $(e,e'n)$ and $(\mu,\mu'n)$ was examined, since there are substantial amounts of these particles in the low energy pion beams (e.g., $\approx$60% $e^-+\mu^-$ in the LEP 60-MeV $\pi^-$ beam). Kuhl and Kneissl[26] have published cross sections for $^{12}C(e^\pm,e^\pm n)^{11}C$ between 26 and 30 MeV, and using a generous linear extrapolation of their data to 120 MeV (same momentum as 50-MeV pions) one obtains $\sigma_e \approx 0.14$ mb. This cross section leads to about 1% $^{11}C$ contribution due to $e^-$ in the 50-MeV $\pi^-$ beam and about a 0.5% contribution due to $e^+$ in the 50-MeV $\pi^+$ beam. Recently the cross section for the $^{12}C(\mu^+,\mu^+n)^{11}C$ reaction at 60 MeV has been measured[27] to be $21\pm4$ $\mu$b. Since 60-MeV muons accompany 50-MeV pions and one can assume that the cross sections for muon reactions with $^{12}C$ are essentially charge independent, we have concluded that in our worst case, namely, 50-MeV $\pi^-$ on $^{12}C$, the contribution to $^{11}C$ production by muons is only 0.05%. Considering the large uncertainties in our low energy cross sections we have chosen to neglect the $^{11}C$ contribution from these lepton-induced reactions.

## III. RESULTS

### A. Measured cross sections

The results are given in Table II, which lists the mean energy and energy spread of the pion beams, the experimental cross section at that energy, and the number of measurements. The excitation functions for the $^{12}C(\pi^\pm,\pi N)^{11}C$ reactions are shown in Fig. 6, and the smooth curves were drawn to fit the data. Table III lists our recom-

TABLE II. Cross section for the $^{12}C(\pi^\pm,\pi N)$ $^{11}C$ reactions.

| $\pi^+$ | | | $\pi^-$ | | |
|---|---|---|---|---|---|
| Energy (MeV) | Cross section (mb) | No. of meas. | Energy (MeV) | Cross section (mb) | No. of meas. |
| 39.9±0.2 | 8.17±2.09 | 1 | 40.0± 0.7 | 6.11±2.62 | 1 |
| 49.9±0.4 | 15.21±1.56 | 4 | 50.0± 0.4 | 8.24±1.86 | 3 |
| 54.8±0.5 | 16.90±3.26 | 1 | 55.0± 0.5 | 8.77±3.33 | 1 |
| 59.9±0.3 | 16.59±3.17 | 1 | 60.0± 0.3 | 9.94±3.52 | 1 |
| 69.6±0.5 | 23.91±3.77 | 1 | 70.0± 1.2 | 18.41±5.64 | 1 |
| 74.5±0.6 | 25.59±2.66 | 2 | 75.0± 0.6 | 23.81±4.83 | 2 |
| 79.8±0.3 | 25.01±3.48 | 1 | 80.0± 0.3 | 22.96±6.21 | 1 |
| 89.6±0.5 | 34.24±3.89 | 1 | 90.0± 0.5 | 33.70±7.80 | 1 |
| 100.6±1.5 | 30.78±1.08 | 5 | 101.3± 2.2 | 35.97±4.16 | 3 |
| 119.7±0.9 | 39.26±1.63 | 2 | 119.5± 2.8 | 45.13±0.99 | 2 |
| 139.6±1.0 | 41.75±1.87 | 2 | 130.0± 1.0 | 60.80±3.10 | 3 |
| 149.5±2.2 | 44.24±1.44 | 3 | 146.3± 3.2 | 58.35±1.88 | 2 |
| 159.6±1.2 | 46.10±1.96 | 2 | 169.5± 3.5 | 67.08±2.13 | 2 |
| 166.9±4.9 | 44.46±1.59 | 4 | 179.9± 1.3 | 73.84±1.92 | 2 |
| 179.6±1.3 | 44.91±1.88 | 2 | 190.8± 5.2 | 66.97±1.52 | 2 |
| 188.3±2.6 | 40.97±0.69 | 2 | 209.5± 2.9 | 69.62±1.11 | 2 |
| 219.6±1.5 | 39.45±2.33 | 1 | 230.0± 7.9 | 65.48±3.57 | 1 |
| 225.6±3.1 | 35.91±1.16 | 2 | 236.8± 5.3 | 59.62±1.58 | 2 |
| 243.3±3.0 | 31.88±0.28 | 2 | 259.5± 3.5 | 57.96±1.27 | 2 |
| 279.5±3.3 | 25.90±0.59 | 2 | 283.6± 5.1 | 48.51±1.19 | 2 |
| 288.3±5.9 | 25.16±0.70 | 3 | 331.1± 6.4 | 37.86±0.95 | 2 |
| 334.1±3.8 | 21.22±0.21 | 3 | 379.0± 6.5 | 29.87±0.86 | 3 |
| 371.0±6.4 | 19.07±0.72 | 4 | 435.1± 8.0 | 23.52±0.74 | 2 |
| 385.8±2.3 | 21.06±1.50 | 4 | 479.5± 5.9 | 23.29±0.71 | 2 |
| 416.2±5.9 | 21.04±4.61 | 4 | 549.5± 9.9 | 18.64±0.73 | 2 |
| 431.2±4.9 | 21.18±0.97 | 1 | 600.0±30.8 | 17.39±0.83 | 1 |
| 470.1±9.1 | 22.52±0.55 | 2 | | | |
| 477.4±5.2 | 22.72±0.51 | 2 | | | |
| 520.6±5.6 | 23.60±1.65 | 1 | | | |

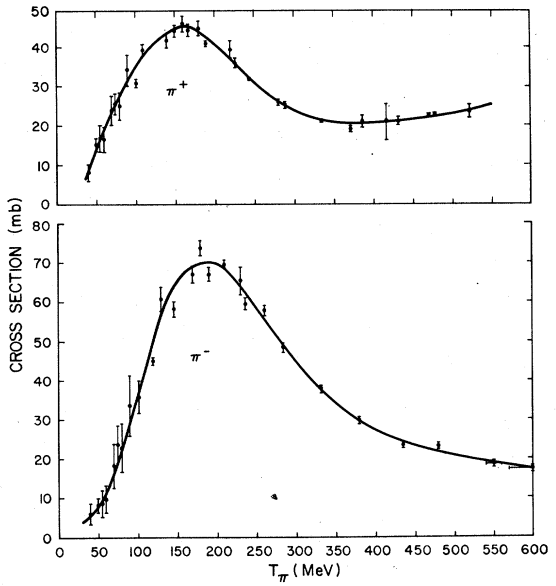


FIG. 6. Absolute cross sections for the $^{12}C(\pi^{\pm},\pi N)^{11}C$ reactions. Smooth curves were drawn through the points to facilitate the extraction of cross sections at energies other than those measured here.

mended values for cross sections read from these curves at 10-MeV intervals from 40 to 250 MeV and at 25-MeV intervals from 275 to 600 MeV. (These intervals are small enough to allow cross sections at other energies to be calculated by linear interpolation without significant error.) The uncertainties associated with the recommended values are derived from a simple averaging of uncertainties in the experimental points for each energy region. Table III also lists the $\sigma(\pi^-)/\sigma(\pi^+)$ ratios calculated from these cross sections.

The results of our measurements are compared in Fig. 7 with those reported in Refs. 2, 9–12, 14, and 28. In the case of the $\pi^-$-induced reactions, the agreement with previous measurements, particularly those by Reeder and Markowitz[9] and by Moinester *et al.*,[12] is excellent. Comparison with both the $\pi^+$ and $\pi^-$ measurements made by Batist *et al.*[14] during the period of our early measurements shows very good agreement from 100 to 180 MeV but significant disagreement from 220 to 295 MeV. No explanation is apparent for their consistently higher cross sections than ours above the (3,3) resonance. Clearly, their $\sigma(\pi^-)/\sigma(\pi^+)$ ratio at 180 MeV of $1.57 \pm 0.05$ is in excellent agreement with our ratio of $1.59 \pm 0.07$.

Comparison of our $\pi^+$ cross sections with earlier measurements show that the agreement with the results of Moinester *et al.* and Reeder and Markowitz is good; however, the cross sections reported by Chivers *et al.*[2] and Hogstrom *et al.*[10]

TABLE III. Interpolated cross sections and ratios for the $^{12}C(\pi^{\pm},\pi N)^{11}C$ reactions.

| $E$(MeV) | $\sigma(\pi^+)$ (mb) | $\sigma(\pi^-)$ (mb) | $\sigma(\pi^-)/\sigma(\pi^+)$ |
|---|---|---|---|
| 40 | 8.8±1.9 | 5.7±2.3 | 0.65±0.30 |
| 50 | 13.7±2.6 | 8.1±2.9 | 0.59±0.24 |
| 60 | 19.0±3.2 | 11.6±3.7 | 0.61±0.22 |
| 70 | 23.6±3.4 | 17.5±4.8 | 0.74±0.23 |
| 80 | 27.6±3.3 | 23.8±5.5 | 0.86±0.22 |
| 90 | 31.5±3.0 | 30.6±5.8 | 0.97±0.21 |
| 100 | 35.0±2.6 | 37.2±5.5 | 1.06±0.18 |
| 110 | 38.0±1.9 | 44.6±4.8 | 1.17±0.14 |
| 120 | 40.4±1.4 | 51.5±3.4 | 1.27±0.10 |
| 130 | 42.3±1.4 | 57.3±1.6 | 1.35±0.06 |
| 140 | 43.7±1.5 | 62.0±1.8 | 1.42±0.06 |
| 150 | 44.6±1.5 | 65.6±1.9 | 1.47±0.07 |
| 160 | 45.1±1.6 | 68.0±2.0 | 1.51±0.07 |
| 170 | 45.0±1.6 | 69.4±2.0 | 1.54±0.07 |
| 180 | 44.0±1.5 | 70.0±2.0 | 1.59±0.07 |
| 190 | 42.6±1.5 | 70.2±2.1 | 1.65±0.08 |
| 200 | 40.9±1.4 | 69.8±2.1 | 1.71±0.08 |
| 210 | 39.0±1.4 | 68.6±2.0 | 1.76±0.08 |
| 220 | 36.9±1.3 | 66.6±2.0 | 1.80±0.08 |
| 230 | 34.7±1.2 | 63.8±1.9 | 1.84±0.08 |
| 240 | 32.7±1.2 | 61.1±1.9 | 1.87±0.09 |
| 250 | 30.8±1.1 | 58.3±1.8 | 1.89±0.09 |
| 275 | 26.9±1.0 | 51.2±1.6 | 1.90±0.09 |
| 300 | 23.7±0.9 | 44.7±1.4 | 1.89±0.09 |
| 325 | 21.8±0.8 | 39.0±1.2 | 1.79±0.09 |
| 350 | 20.9±0.8 | 34.4±1.1 | 1.65±0.08 |
| 375 | 20.6±0.8 | 30.4±1.0 | 1.48±0.08 |
| 400 | 20.7±0.8 | 27.3±0.9 | 1.32±0.07 |
| 425 | 21.1±0.8 | 25.0±0.8 | 1.18±0.06 |
| 450 | 21.6±0.9 | 23.4±0.8 | 1.08±0.06 |
| 475 | 22.1±0.9 | 22.1±0.8 | 1.00±0.05 |
| 500 | 23.0±0.9 | 21.0±0.7 | 0.91±0.05 |
| 525 | 24.1±1.0 | 20.1±0.7 | 0.83±0.05 |
| 550 | 25.6±1.1 | 19.0±0.7 | 0.74±0.04 |
| 575 | ... | 18.4±0.7 | ... |
| 600 | ... | 17.5±0.6 | ... |

are in poor agreement with ours. An underestimation of the proton contamination in the $\pi^+$ beams used by Chivers *et al.* could account for their $\pi^+$ cross sections being too large; the fact that their $\pi^-$ results agree with ours lends support to this conjecture.

### B. Analysis of uncertainties

The uncertainties in each component of the cross-section calculation for each target were combined as described below to obtain an uncertainty for each calculated cross section. Multiple determinations and their uncertainties were then averaged to arrive at a cross section and an uncertainty for each energy and pion charge. A sample standard deviation was also calculated for the same set of multiple determinations, and the larger of that standard deviation and the former

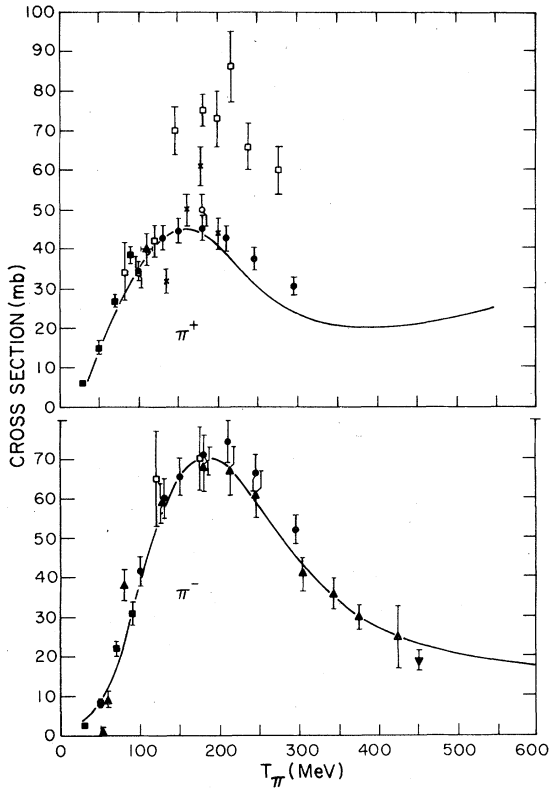


FIG. 7. Comparison with other measurements. The solid curves are the same as those in Fig. 6. Symbols: □-Ref. 2, ▲-Ref. 9, ×-Ref. 10, ○-Ref. 11, ■-Ref. 12, ●-Ref. 14, ▼-Ref. 28.

uncertainty was used. The weighted sample standard deviation was larger than the combined individual uncertainties in about 17% of the cases, indicating that our estimates of the uncertainties of the individual measurements were consistent.

Only the half-life and the target density were assumed to be known precisely. Analysis of the decay curves provided an uncertainty in end-of-bombardment (EOB) disintegration rates, and the TOF and $dE/dx$ analyses gave uncertainties in beam contamination figures. Uncertainties in the pion fluences were calculated by assuming that there was an uncertainty of ±50% in the accidental coincidence correction to the rate, reflecting the compromise made between the 1-bunch and 2-bunch corrections (see Sec. II B above). The length of the bombardment was usually determined from the intensity monitor, and so the uncertainty in that time was directly proportional to the quality of the calibration of the intensity monitor.

The general relation for the uncertainty calculation is

$$\rho_C^2 = \rho_A^2 + \rho_\phi^2 + \rho_\epsilon^2 ,$$

where

$C$ = cross section,
$A$ = EOB activity (disintegrations per minute),
$\phi$ = total fluence, corrected for beam contamination and true coincidence losses,
$\epsilon = t/[1 - \exp(-\lambda t)]$,
$t$ = length of bombardment,
$\lambda$ = decay constant of $^{11}C$ ($t_{1/2}$ = 20.4 min), and
$\rho$ = relative uncertainty (e.g., $\rho_A = \sigma_A/A$, where $\sigma_A$ = uncertainty in $A$).

The method of arriving at $\rho_A$ and $\rho_\phi$ follows directly from the preceding paragraph. However, $\rho_\epsilon$ is derived from $\partial\epsilon/\partial t$ [that is, $\rho_\epsilon = \sigma_\epsilon/\epsilon$ and $\sigma_\epsilon^2 = (\partial\epsilon/\partial t)^2$] and its final form is

$$\rho_\epsilon = \sigma_t\left(\frac{1}{t} - \frac{e^{-\lambda t}}{1 - e^{-\lambda t}}\right).$$

An examination of this expression shows that for large $t$(>2.5 h) $\rho_\epsilon \approx \sigma_t/t$ but that for smaller $t$, $\rho_\epsilon < \sigma_t/t$. (At $t$ = 400 sec, $\rho_\epsilon \approx 0.1\ \sigma_t/t$ and at $t$ = 2200 sec, $\rho_\epsilon \approx 0.5\ \sigma_t/t$.) This source of uncertainty was usually negligible and was only included in the calculations in those few cases where $\sigma_t/t$ was > 0.005.

The uncertainty in the measured $(p,pn)$ cross sections were also taken into account in those cases where protons were observed to be present in the beam. Since those uncertainties were on the order of 6% and since the proton contamination in the beam was at most 19% at the highest $\pi^+$ energy, the resulting uncertainty is less than 1.2% in all cases.

## IV. DISCUSSION

The most striking features of these measured $^{12}C(\pi^\pm, \pi N)^{11}C$ excitation functions are the following. (a) The ratio for $\sigma_{\pi^-}/\sigma_{\pi^+}$ at 180 MeV is 1.59 ± 0.07, in contrast to both the previously measured value of 1.0 ± 0.1[2] and the expected free-particle ratio of 3.0.[29] (b) The peak in the (3,3) resonance for $\pi^-$ on carbon is shifted upward in energy and for $\pi^+$ it is shifted downward, relative to the free-particle resonances at 180 MeV.[29] These shifts in the resonances obviously result in the $\sigma_{\pi^-}/\sigma_{\pi^+}$ ratio varying with pion energy. (c) The widths of the resonances for carbon are noticeably greater than the widths of the free-particle resonances, presumably due to the Fermi motion of the $^{12}C$ nucleons. (d) The $\pi^+$ cross section above about 350 MeV rises, due to the onset of the $T$ = 1/2 free-nucleon resonance at 600 MeV.

The most successful effort to date at a theoretical computation of results corresponding to those presented here has been made by Sternheim and Silbar.[30] Their model, which grew out of ideas presented earlier by Hewson,[3] uses a semiclassical transport model to estimate the probability

that a nucleon struck by the incoming pion will undergo charge exchange before leaving the nucleus. For the $^{12}C \xrightarrow{\pi^-} {}^{11}C$ reaction, the depletion of the $^{11}C$ product by charge exchange after an initial $\pi^- - n$ collision exceeds the $^{11}C$ enchancement by charge exchange after a $\pi^- - p$ collision, producing a net lowering of the cross section. Exactly the opposite occurs for $\pi^+$ projectiles. The net effect of this charge exchange process is a large reduction in the $\sigma_{\pi^-}/\sigma_{\pi^+}$ ratio from the impulse approximation ratio of 3.

According to Sternheim and Silbar, the ratio $R$ of the $\pi^-$ to $\pi^+$ cross section for a $Z=N$ target nucleus based on the impulse approximation but modified by the nucleon charge exchange probability $P$ can be written as

$$R=\frac{\sigma_{\pi^-}}{\sigma_{\pi^+}}=\frac{(1-P)\sigma_{\pi^- n}+P\sigma_{\pi^- p\to\pi^- p}}{(1-P)\sigma_{\pi^+ n}+P\sigma_{\pi^+ p}}$$
$$\approx\frac{9-8P}{3+6P},$$

where the approximate form includes only the $(\frac{3}{2},\frac{3}{2})$ amplitude. They proceeded to show that the charge exchange probability $P$ is an exponential function of the nucleon charge exchange cross section and the average path length of the struck nucleon, both of which are functions of the energy of the struck nucleon or, in turn, the incident pion energy. The experimental nucleon charge exchange cross section, which is the dominant factor, drops rapidly with energy in the range of 14 to 40 MeV (Ref. 31) and, therefore, $P$ also decreases with increase in pion kinetic energy.

This energy dependence of the charge exchange probability can provide a qualitative explanation for our observed peak shifts. Since the probability decreases sharply as the pion energy increases, the depletion of the $^{11}C$ product by the $n\to p$ charge exchange in the case of the $\pi^-$-induced reactions is greater at lower energies, thereby producing a shift in the peak of the excitation function toward higher energy. Since the converse situation prevails for the $\pi^+$-induced reactions, the result is a downward shift of the peak.

Sternheim and Silbar calculated the ratio $R$ as a function of pion energy employing the exact expression shown above. It was necessary for them to normalize their ratio function to our experimental value at one energy; they chose 180 MeV. The comparison between their calculated ratio curve and the experimental curve is shown in Fig. 8. The agreement over the applicable energy range is remarkably good. The reason the curves do not coincide at 180 MeV is because our experimental ratio has been raised slightly from the

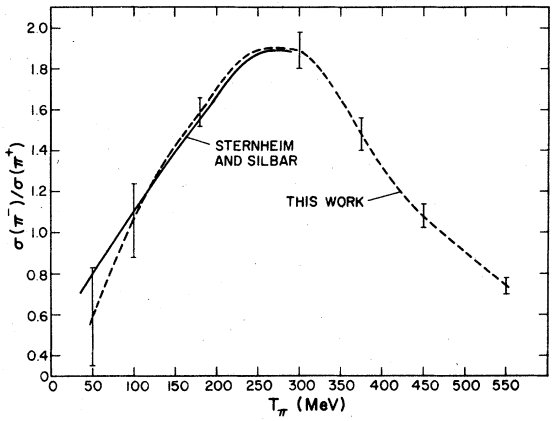


FIG. 8. Comparison of experimental and theoretical $\sigma(\pi^-)/\sigma(\pi^+)$ ratios. Solid curve is from Sternheim and Silbar's charge-exchange model (Ref. 30). Dashed curve is a smoothed version of the ratio data from Table III.

earlier ratio (to which they normalized) as a result of more measurements and further refinements in the analysis of the data. It would appear that charge exchange of the outgoing nucleons as estimated semiclassically can account for the large differences between the observed neutron-knock-out ratios and the impulse-approximation predictions.

Additionally, Sternheim and Silbar proceeded to calculate the actual nucleon knock-out cross sections. They assumed that this reaction channel was a constant fraction of the total pion-nucleus reaction cross section times a threshold factor.

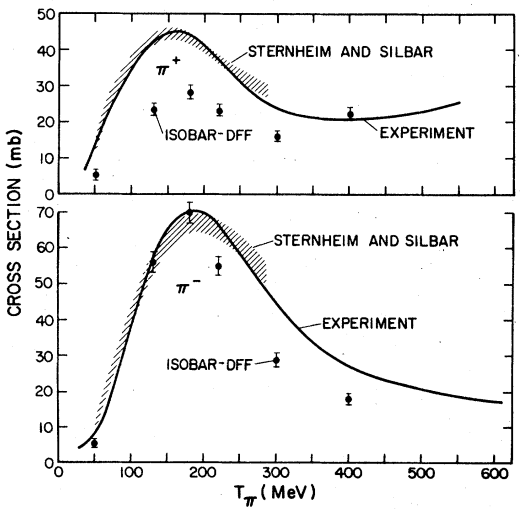


FIG. 9. Comparison with theories. The solid curves are the same as those in Fig. 6. The points are calculated with the intranuclear cascade (ISOBAR) and evaporation (DFF) codes (Refs. 35, 36, and 34, respectively). The dashed bands represent the charge exchange model of Sternheim and Silbar (Ref. 30).

By using experimental $\pi^-$-$^{12}$C cross sections[32] and their energy-dependent values for $R$, they determined the bands of neutron-knock-out cross section values shown on Fig. 9. The width of the bands reflects the experimental errors in the total reaction cross sections. Again, the agreement with our experimental excitation functions is rather remarkable.

Another theoretical model was examined for comparison with the results of this study. The two-stage model involving intranuclear cascade followed by evaporation processes (VEGAS[33] plus DFF[34]) has been successfully employed to predict yields of spallation products from intermediate energy proton-induced reactions. The ISOBAR[35,36] version of VEGAS was developed to treat the interactions of fast pions with complex nuclei. In this model the incident pion can either simply scatter inelastically off a nucleon or, if its energy is near the (3,3) resonance value, scatter resonantly with the formation of a pion-nucleon isobar or delta. This isobar can then either decay back into a pion and nucleon or collide with another target nucleon resulting in two nucleons which gain the rest mass energy of the pion. This latter process provides a mechanism for pion absorption. The ISOBAR model has met with considerable success in predicting the spallation-product yields from the interactions of Cu with 50-, 100-, 190-, and 350-MeV pions[37] and in predicting the spectra of emitted protons[38] from 100-MeV pions on Al and 220-MeV pions on $^{62}$Ni.

The $^{11}$C production cross sections as calculated with the ISOBAR and DFF codes are shown in Fig. 9. While the calculated values for the $\pi^-$ reaction agree very well with the experimental cross sections from 50 to 180 MeV, they drop more rapidly above the (3,3) resonance. The narrower resonance resulting from these calculated values suggests that in this model the interactions are more peripheral than the measured resonance would indicate.

The calculated values for the $\pi^+$ reaction are considerably lower than the measured cross sections, except at 400 MeV where the influence of the $T=1/2$ resonance at 600 MeV appears to have a strong effect.[35] Obviously the ratio of the cross sections at 180 MeV as calculated by ISOBAR-DFF, $\sigma_{\pi^-}/\sigma_{\pi^+}=2.4$, is much larger than the measured ratio $(1.59\pm0.07)$. The reason for this serious discrepancy in the calculated $\pi^+$ reaction cross sections is not at all understood. It is particularly puzzling in view of the fact that the basic physics, including nucleon charge exchange, in the ISOBAR model is essentially the same as in the approach taken by Sternheim and Silbar.[30] It has been conjectured[39] that the ISOBAR model probably neglects some important quantum mechanical coherence in the nucleon charge exchange process. The puzzle is compounded by the fact that Kaufman *et al.*[40] found that for a heavy target nucleus (Au) the neutron removal cross section ratio, $\sigma_{\pi^-}/\sigma_{\pi^+}$, as calculated with ISOBAR-DFF, gives good agreement with their measured ratio whereas the value predicted with the nucleon charge exchange model[30] gives poor agreement.

## ACKNOWLEDGMENTS

We gratefully acknowledge the work of the LAMPF technical staff and operating crews for enabling us to carry out these numerous target irradiations. Our gratitude is expressed to J. N. Ginocchio and R. R. Silbar for many helpful discussions and calculations relevant to our experimental results. We thank G. A. Cowan and J. E. Sattizahn for their encouragement and support of this work. This work was performed under the auspices of the U. S. Department of Energy.

## APPENDIX: ACCIDENTAL COINCIDENCE LOSS CORRECTIONS FOR A TIME-STRUCTURED BEAM[41]

In a time-structured beam with micropulses $\Delta t$ nsec apart, the probability that a micropulse will contain $n$ particles is given by the Poisson distribution

$$P_n(a)=\frac{a^n}{n!}e^{-a}, \tag{A1}$$

where $a$ is the average number of particles per micropulse. Assume that the resolving time $\tau$ of the counting circuit allows particles separated by $\Delta t$ to be counted but that multiple particles in a micropulse are counted as one particle. This will be referred to as "one-bunch resolution." If $a$ is independent of time, then the number of counts $N$ after $m$ bunches will be

$$N=m(1-e^{-a}), \tag{A2}$$

since $(1-e^{-a})$ is the probability that a micropulse contains at least one particle. But in $m$ bunches the total number of particles $N_p$ is $N_p=ma$, so that the correction to $N$ is simply $N_p-N=m(a-1+e^{-a})$. In order to determine $a$, one may measure the delayed self-coincidences $N_s$ ($C_1\tilde{C}_2$ in Fig. 1). The number of delayed self-coincidences $N_s$ is just the probability of getting a count $(1-e^{-a})$ times the probability of getting a count in some other micropulse, which is also $(1-e^{-a})$ since they are independent. Thus, after $m$ micropulses the number of self-coincidences is

$$N_s=m(1-e^{-a})^2. \tag{A3}$$

From (A2) and (A3), we obtain $N^2/N_s = m$ and $a = \ln[N/(N-N_s)]$. Using $N_p = ma$, we get the one-bunch resolution formula

$$N_p = \frac{N^2}{N_s}\ln\left(\frac{N}{N-N_s}\right). \quad \text{(A4)}$$

Note that for small $a$, this reduces to $N_p \approx N + N_s/2$.

If, however, $\tau$ is such that particles separated by $\Delta t$ cannot be resolved but alternate micropulses can be resolved, i.e., $\Delta t < \tau < 2\Delta t$, the situation will be referred to as "two-bunch resolution." In this case we will assume that the electronics are paralyzed after a count, so a second count in the next bunch is not recorded. As before, the probability of finding at least one particle in a micropulse is $(1 - e^{-a})$, and the probability of two adjacent bunches each having at least one particle is $(1 - e^{-a})^2$, which is also the probability of missing a count. Thus, the number of counts recorded after $m$ bunches is

$$N = m[(1 - e^{-a}) - (1 - e^{-a})^2]. \quad \text{(A5)}$$

Similarly, the number of delayed self-coincidences is

$$N_s = m[(1 - e^{-a}) - (1 - e^{-a})^2]^2. \quad \text{(A6)}$$

Combining (A5) and (A6) we get the two-bunch resolution formula

$$N_p = \frac{N^2}{N_s}\ln\left[\frac{2}{1 \pm (1 - 4N_s/N)^{1/2}}\right]. \quad \text{(A7)}$$

Note that for small $a$, this reduces to $N_p \approx N + 3N_s/2$.


[1]The notation $^{12}C(\pi^{\pm},\pi N)^{11}C$ is used in this paper to designate the production of $^{11}C$ from $^{12}C$ by $\pi^{\pm}$ mesons irrespective of mechanism.

[2]D. T. Chivers, E. M. Rimmer, B. W. Allardyce, R. C. Witcomb, J. J. Domingo, and N. W. Tanner, Nucl. Phys. A126, 129 (1969); D. T. Chivers, J. J. Domingo, E. M. Rimmer, R. C. Witcomb, B. W. Allardyce, and N. W. Tanner, Phys. Lett. 26B, 573 (1968).

[3]D. H. Wilkinson, J. Phys. Soc. Japan Suppl. 24, 469 (1968).

[4]R. Seki, Nuovo Cimento 9A, 235 (1972).

[5]V. M. Kolybasov, Phys. Lett. 27B, 3 (1972).

[6]V. M. Kolybasov and N. Ya. Smorodinskaya, Phys. Lett. 30B, 11 (1969).

[7]D. Robson, Ann. Phys. (N.Y.) 71, 277 (1972).

[8]P. W. Hewson, Nucl. Phys. A133, 659 (1969).

[9]P. L. Reeder, doctoral thesis, University of California Report No. UCRL-10531 (1962), published as P. L. Reeder and S. S. Markowitz, Phys. Rev. 133, B639 (1964).

[10]K. R. Hogstrom, B. W. Mayes, L. Y. Lee, J. C. Allred, C. Goodman, G. S. Mutchler, C. R. Fletcher, and G. C. Phillips, Nucl. Phys. A215, 598 (1973).

[11]M. V. Yester, A. A. Caretto, M. Kaplan, P. J. Karol, and R. L. Klobuchar, Phys. Lett. 45B, 327 (1973).

[12]M. A. Moinester, M. Zaider, J. Alster, D. Ashery, S. Cochavi, and A. I. Yavin, Phys. Rev. C 8, 2039 (1973).

[13]B. J. Dropesky, G. W. Butler, C. J. Orth, R. A. Williams, G. Friedlander, M. A. Yates, and S. Kaufman, Phys. Rev. Lett. 34, 821 (1975).

[14]L. H. Batist, V. D. Vitman, V. P. Koptev, M. M. Makarov, A. A. Naberezhnov, V. V. Nelyubin, G. Z. Obrant, V. V. Sarantsev, and G. V. Scherbakov, Nucl. Phys. A254, 480 (1975).

[15]R. L. Burman, R. Fulton, and M. Jacobson, Nucl. Instrum. Methods 131, 29 (1975).

[16]R. D. Werbeck and R. J. Macek, IEEE Transactions Nucl. Sci. 22, 1598 (1975).

[17]Formerly produced by Pilot Chemicals Division, New England Nuclear Corp., Watertown, Mass., but currently manufactured by Nuclear Enterprises, Inc., San Carlos, Calif.

[18]MECL=Motorola Emitter Coupled Logic; the NIM units were fabricated by the Physics Division, Lawrence Berkeley Laboratory.

[19]W. R. Busing and H. A. Levy, Oak Ridge National Lab. Report No. ORNL-TM-271 (1962).

[20]J. T Routti and S. G. Prussin, Nucl. Instrum. Methods 72, 125 (1969).

[21]R. J. Macek, private communication.

[22]J. B. Cumming, A. M. Poskanzer, and J. Hudis, Phys. Rev. Lett. 6, 484 (1961).

[23]L.P. Remsberg, Annu. Rev. Nucl. Sci. 17, 347 (1967).

[24]J. B. Cumming, USAEC Report No. NAS-NA-3017, p. 25 (1963).

[25]J. B. Cumming, Annu. Rev. Nucl. Sci. 13, 261 (1963).

[26]G. Kuhl and U. Kneissl, Nucl. Phys. A195, 559 (1972); F. J. Kline and E. Hayward, Phys. Rev. C 17, 1531 (1978).

[27]C. J. Orth, M. W. Johnson, J. D. Knight, and K. Wolfsberg, LAMPF Experiment 331. A report is in preparation for publication.

[28]A. M. Poskanzer and L. P. Remsberg, Phys. Rev. 123, B779 (1964).

[29]A. A. Carter, J. R. Williams, D. V. Bugg, P. J. Bussey, and D. R. Dance, Nucl. Phys. B26, 445 (1971).

[30]M. M. Sternheim and R. R. Silbar, Phys. Rev. Lett. 34, 824 (1975).

[31]J. P. Scalon, G. H. Stafford, J. J. Thresher, P. H. Bowen, and A Langsford, Nucl. Phys. 41, 401 (1963).

[32]F. Binon, P. Duteil, J. P. Garron, J. Gorres, L. Hugon, J. P. Peigneux, C. Schmit, M. Spighel, and J. P. Stroot, Nucl. Phys. B17, 168 (1970).

[33]N. Metropolis, R. Bivins, M. Storm, A. Turkevich, J. M. Miller, and G. Friedlander, Phys. Rev. 110, 204 (1958); K. Chen, Z. Fraenkel, G. Friedlander, J. R. Grover, J. M. Miller, and Y. Shimamoto, *ibid.* 166,

949 (1968).
[34]I. Dostrovsky, Z. Fraenkel, and G. Friedlander, Phys. Rev. 116, 683 (1959).
[35]G. D. Harp, K. Chen, G. Friedlander, Z. Fraenkel, and J. M. Miller, Phys. Rev. C 8, 581 (1973).
[36]J. N. Ginocchio, Phys. Rev. C 17, 195 (1978).
[37]C. J. Orth, B. J. Dropesky, R. A. Williams, G. C. Giesler, and J. Hudis, Phys. Rev. C 18, 1426 (1978).
[38]H. E. Jackson, S. B. Kaufman, L. Meyer-Schützmeister, J. P. Schiffer, S. L. Tabor, S. E. Vigdor, J. N. Worthington, L. L. Rutledge, R. E. Segal, R. L. Burman, P. A. M. Gram, R. P. Redwine, and M. A. Yates, Phys. Rev. C 16, 730 (1977).
[39]R. R Silbar, J. N. Ginocchio, and M. M. Sternheim, Phys. Rev. C 18, 2785 (1978).
[40]S. B. Kaufman, E. P. Steinberg, and G. W. Butler (unpublished).
[41]This analysis procedure was provided in a private communication from W. K. McFarlane.